

EXPLORING THE CONVECTIVE CORE OF THE HYBRID δ SCUTI- γ DORADUS STAR COROT 100866999 WITH ASTEROSEISMOLOGY

XINGHAO CHEN^{1,2}, YAN LI^{1,2,3,4}, AND XIAOBIN ZHANG⁵

Draft version November 19, 2019

ABSTRACT

We computed a grid of theoretical models to fit the δ Scuti frequencies of CoRoT 100866999 detected earlier from the CoRoT timeserials. The pulsating primary star is determined to be a main sequence star with a rotation period of $4.1^{+0.6}_{-0.5}$ days, rotating slower than the orbital motion. The fundamental parameters of the primary star are determined to be $M = 1.71^{+0.13}_{-0.04} M_{\odot}$, $Z = 0.012^{+0.004}_{-0.000}$, $f_{\text{ov}} = 0.02^{+0.00}_{-0.02}$, $T_{\text{eff}} = 8024^{+249}_{-297}$ K, $L = 11.898^{+2.156}_{-1.847} L_{\odot}$, $\log g = 4.166^{+0.013}_{-0.002}$, $R = 1.787^{+0.040}_{-0.016} R_{\odot}$, and $X_{\text{c}} = 0.488^{+0.011}_{-0.020}$, matching well those obtained from the eclipsing light curve analysis. Based on the model fittings, p_1 and p_5 are suggested to be two dipole modes, and p_3 , p_4 , p_6 , and p_7 to be four quadrupole modes. In particular, p_4 and p_7 are identified as two components of one quintuplet. Based on the best-fitting model, we find that p_1 is a g mode and the other nonradial modes have pronounced mixed characters, which give strong constraints on the convective core. Finally, the relative size of the convective core of CoRoT 100866999 is determined to $R_{\text{conv}}/R = 0.0931^{+0.0003}_{-0.0013}$.

Subject headings: Asteroseismology - binaries: eclipsing - stars: individual (CoRoT 100866999) - stars: oscillations - stars: variables: δ Scuti - stars: variables: γ Doradus

1. INTRODUCTION

The δ Scuti (Campbell & Wright 1900) and γ Dor variables (Kaye et al. 1999) are two classes of late A- and early F-type stars. δ Scuti stars mainly pulsate in low-order radial and nonradial modes with typical periods in the range of 0.02-0.25 days (Breger 2000), which are driven by the κ mechanism (Baker & Kippenhahn 1962, 1965; Zhevakin 1963; Li & Stix 1994) operating in the second partial ionization zone of helium (Chevalier 1971; Dupret et al. 2004; Grigahcène et al. 2005). Due to the low radial order, oscillations of δ Scuti stars are not in the asymptotic regime, while their pulsation patterns still exhibit regularities (e.g., Paparó et al. 2013, 2016). These regularities also include the scaling relation between the large frequency separation and the mean density of the star (Suárez et al. 2014; García Hernández et al. 2015, 2017), the amplitude modulation (Bowman & Kurtz 2014; Barceló Forteza et al. 2015; Bowman et al. 2016), and the empiric relation between the frequency of the maximum oscillation power ν_{max} and the effective temperature T_{eff} (Barceló Forteza et al. 2018). γ Dor stars pulsate in g-mode oscillations driven by the convective blocking mechanism, which operates in the outer convective zone (Guzik et al. 2000; Dupret et al. 2004, 2005; Grigahcène et al. 2005). Their periods are rela-

tively longer, i.e., between 0.3 days and 3 days. The g modes of γ Dor stars and their departure from the constant period spacing allow us to probe the interiors of the star, such as chemical mixing (Miglio et al. 2008) and rotation (Van Reeth et al. 2015, 2016, 2018).

In the Hertzsprung-Russel diagram, the instability strips of δ Scuti and γ Dor stars largely overlaps with each other (Balona 2011; Henry et al. 2011; Uytterhoeven et al. 2011; Xiong et al. 2016). Xiong et al. (2016) showed that most of the pulsating variables in the δ Sct- γ Dor instability strip are very likely hybrids that pulsate in both p and g modes. Moya et al. (2017) found that the boundary of δ Scuti and γ Dor pulsations depends on the temperature. The first such hybrid star was detected from the ground by Henry & Fekel (2005). Thanks to the space missions MOST (Walker et al. 2003), CoRoT (Baglin et al. 2006), and Kepler (Borucki et al. 2010), the hybrid behavior is found to be common for A- and F-type stars (Grigahcène et al. 2010; Balona et al. 2015), and a large number of hybrid δ Sct- γ Dor pulsators have been detected and precisely observed, such as CoRoT 1057330033 (Chapellier et al. 2012), KIC 11145123 (Kurtz et al. 2014), and KIC 9244992 (Saio et al. 2015). The hybrid pulsators are very important and promising objects for the study of the stellar structure, since presence of p- and g-modes allow us probe properties of the star from the envelope to the core.

CoRoT 100866999 is an eclipsing binary observed from May 16 to October 5 in 2007 ($\Delta T = 142$ days) during CoRoT's first long run targeting the Galactic center (LRc01). Sarro et al. (2013) obtained an effective temperature of 7700 ± 400 K using low-resolution spectroscopy observed with the Giraffe multi-object spectrograph installed at VLT at ESO in Chile. Chapellier & Mathias (2013) analysed the eclipsing light curve, and determined physical parameters of the pulsating primary star as $M_1 = 1.80 \pm 0.2 M_{\odot}$, $R_1 = 1.90 \pm 0.2 R_{\odot}$, $\log g_1$

¹ Yunnan Observatories, Chinese Academy of Sciences, P.O. Box 110, Kunming 650216, China; chenxinghao@ynao.ac.cn; ly@ynao.ac.cn

² Key Laboratory for Structure and Evolution of Celestial Objects, Chinese Academy of Sciences, P.O. Box 110, Kunming 650216, China

³ University of Chinese Academy of Sciences, Beijing 100049, China

⁴ Center for Astronomical Mega-Science, Chinese Academy of Sciences, 20A Datun Road, Chaoyang District, Beijing, 100012, China

⁵ Key Laboratory of Optical Astronomy, National Astronomical Observatories, Chinese Academy of Sciences, Beijing, 100012, China; xzhang@bao.ac.cn

$= 4.1 \pm 0.1$, $T_{\text{eff},1} = 7300 \pm 2500$ K, and those of the secondary star as $M_2 = 1.1 \pm 0.2 M_{\odot}$, $R_2 = 0.9 \pm 0.2 R_{\odot}$, $\log g_2 = 4.6 \pm 0.1$, $T_{\text{eff},2} = 5400 \pm 430$ K, respectively. Besides, they extracted 8 independent δ Scuti frequencies in the domain [16.25; 26.67] days $^{-1}$ and 63 independent γ Dor frequencies in the domain [0.30; 3.61] days $^{-1}$ (Table 2 of Chapellier & Mathias (2013)). Moreover, they identified 22 γ Dor frequencies as g modes of $\ell = 1$ with successive radial orders due to their nearly constant period interval.

Sánchez Arias et al. (2017) had carried out detailed asteroseismic modelling for CoRoT 100866999. However, their asteroseismic parameters deviate from the results of the eclipsing analysis given by Chapellier & Mathias (2013). In general, the component stars in binaries always rotate along with their orbital motion. The stellar rotation will result in each nonradial oscillation with the spherical harmonic index ℓ splitting into $2\ell + 1$ different frequencies, thus effects of rotation on oscillations should be included. In this work, we extend the work of Sánchez Arias et al. (2017), and perform a more comprehensive asteroseismic analysis for CoRoT 100866999. The details of input physics are presented in Section 2, and model grids are elaborated in Section 3. We introduce our fitting results in Section 4 and discuss them in Section 5. Finally, we conclude the main results of this work in Section 6.

2. INPUT PHYSICS

The stellar evolution code Modules for Experiments in Stellar Astrophysics (MESA), which was developed by Paxton et al. (2011, 2013, 2015, 2018), is used to compute evolutionary and pulsational models. In particular, the submodule called "pulse_adipls" in version 10398 is used to generate stellar evolutionary models (Paxton et al. 2011, 2013, 2015, 2018), and calculate adiabatic frequencies of their radial and nonradial modes (Christensen-Dalsgaard 2008).

In our work, the 2005 update of the OPAL equation of state tables (Rogers & Nayfonov 2002) are adopted. The OPAL opacity tables of Iglesias & Rogers (1996) for high temperatures region and tables of Ferguson et al. (2005) for low temperatures region are used. The initial ingredient in metallicity is assumed to be identical to that of the sun (Asplund et al. 2009). The classical mixing length theory of Böhm-Vitense (1958) with $\alpha = 1.90$ (Paxton et al. 2011) is used in the convective region. For the overshooting mixing of the convective core, we adopt an exponentially decaying prescription and introduce an overshooting mixing diffusion coefficient

$$D_{\text{ov}} = D_0 \exp\left(\frac{-2z}{f_{\text{ov}} H_p}\right) \quad (1)$$

(Freytag et al. 1996; Herwig 2000). In equation (1), D_0 is the diffusion mixing coefficient near the edge of the convective core, z the distance into radiative zone away from the edge, H_p the pressure scale height, and f_{ov} an adjustable parameters describing the efficiency of the overshooting mixing. In our calculations, the lower limit of the diffusion coefficient is set to be $D_{\text{ov}}^{\text{limit}} = 1 \times 10^{-2}$ cm 2 s $^{-1}$, below which overshooting shuts off. In addition, effects of the stellar rotation, the element diffusion, and magnetic fields on the stellar structure and evolution are

not included in this work.

3. GIRD OF STELLAR MODELS

The evolutionary track and the interior structure of a star depend on the initial stellar mass M , initial chemical ingredient (X , Y , and Z), and the overshooting parameter f_{ov} . In our work, the initial helium abundance is set to be $Y = 0.249 + 1.33Z$ (Li et al. 2018), as a function of the metallicity Z , thus the stellar structure and evolution can be completely determined by M , Z and f_{ov} . In our work, we consider stellar masses M between $1.50 M_{\odot}$ and $2.20 M_{\odot}$ with a step of $0.01 M_{\odot}$, and metallicities Z between 0.005 to 0.030 with a step of 0.001. These values of Z corresponds to the range of [Fe/H] from -0.4 to 0.4 according to

$$[\text{Fe}/\text{H}] = \log\left(\frac{Z}{X}\right) - \log\left(\frac{Z}{X}\right)_{\odot}, \quad (2)$$

where we adopt the value of $(Z/X)_{\odot} = 0.0181$ (Asplund et al. 2009). For the overshooting mixing, we also adopt four different cases: no overshooting ($f_{\text{ov}} = 0$), moderate overshooting ($f_{\text{ov}} = 0.01$), intermediate overshooting ($f_{\text{ov}} = 0.02$), and extreme overshooting ($f_{\text{ov}} = 0.03$).

Each star in the grid is computed from the zero-age main sequence to the post-main sequence stage. Figure 1 depicts a set of evolutionary tracks of stars with $Z = 0.012$, $f_{\text{ov}} = 0.02$, and M ranging from $1.50 M_{\odot}$ to $2.20 M_{\odot}$ in a interval of $0.01 M_{\odot}$. The two dotted lines in Figure 1 corresponds to the constraint of the effective temperature $7000 \text{ K} < T_{\text{eff}} < 8400 \text{ K}$ (Chapellier & Mathias 2013; Sarro et al. 2013). For theoretical models meeting with the constraint, we calculate its frequencies of radial oscillations ($\ell = 0$) and nonradial oscillations with $\ell = 1$ and $\ell = 2$.

Besides, following works of Chen & Li (2018, 2019), we consider the rotation period P_{rot} between 0 day and 10 days with a step of 0.1 days, as the fourth adjustable parameter. For a given P_{rot} , each nonradial oscillation mode will split into $2\ell + 1$ different frequencies according to

$$\nu_{\ell,n,m} = \nu_{\ell,n} + m\delta\nu_{\ell,n} = \nu_{\ell,n} + \beta_{\ell,n} \frac{m}{P_{\text{rot}}} \quad (3)$$

(Saio 1981; Dziembowski & Goode 1992; and Aerts et al. 2010), where $\delta\nu_{\ell,n}$ is the splitting frequency, R is the present radius of the star, and $\beta_{\ell,n}$ is the rotational parameter that determines the size of rotational splitting. The general expression of $\beta_{\ell,n}$ for a uniformly rotating star is deduced to be

$$\beta_{\ell,n} = \frac{\int_0^R (\xi_r^2 + L^2 \xi_h^2 - 2\xi_r \xi_h - \xi_h^2) r^2 \rho dr}{\int_0^R (\xi_r^2 + L^2 \xi_h^2) r^2 \rho dr} \quad (4)$$

(Aerts et al. 2010), where ξ_r and ξ_h are the radial displacement and the horizontal displacement respectively, ρ is the local density, and $L^2 = \ell(\ell + 1)$. According to equation (3), each oscillation mode of $\ell = 1$ splits into three different frequencies, forming a triplet. Each oscillation mode of $\ell = 2$ splits into five different frequencies, forming a quintuplet.

4. FITTING RESULTS OF COROT 100866999

Table 1 lists the eight independent δ Scuti frequencies obtained by Chapellier & Mathias (2013). The frequency

F is the largest-amplitude mode, almost 20 times larger than those of other δ Scuti frequencies. Besides, the period ratio of p_2 and F is 0.776, which equals the well known period ratio 0.772 between the fundamental radial mode and the radial first overtone mode (Fitch 1981; Poretti et al. 2005). In general, the component stars in eclipsing binaries always rotate along with their orbital motion. Suárez et al. (2006) investigated effects of rotation on period ratios of radial modes, and found that the difference of period ratios remains around 10^{-3} for rotational velocities up to 50 km s^{-1} . Moreover, Chapellier & Mathias (2013) found that the radial fundamental mode F corresponds to an absolute magnitude $M_v = 2.4$ mag and an A8V spectral type for the primary star according to the period-luminosity relation of Templeton et al. (2002). These values match well the parameters obtained from the eclipsing light curve fit. Therefore, we use F as the fundamental radial mode and p_2 as the radial first overtone mode in our calculations.

To find the optimal model to observations, we compare model frequencies with the observed frequencies F , p_1 , p_2 , p_3 , p_4 , p_5 , p_6 , and p_7 according to

$$S^2 = \frac{1}{k} \sum (|\nu_{\text{mod},i} - \nu_{\text{obs},i}|^2), \quad (5)$$

where $\nu_{\text{obs},i}$ represents the observed frequency, $\nu_{\text{mod},i}$ represents its corresponding model frequency, and k is the number of the observed frequencies. Frequencies p_1 , p_3 , p_4 , p_5 , p_6 , and p_7 are not identified in advanced, thus theoretical frequencies nearest to them are regarded as their possible model counterparts.

Figures 2 and 3 show plots of resulting S_m^2 versus various physical parameters. Each circle in the figures represents one minimum value of S^2 along one evolutionary track. We denote the minimum value with S_m^2 . In the figures, circles in black, blue, red, and green correspond to theoretical models with $f_{\text{ov}} = 0, 0.01, 0.02$, and 0.03 , respectively. The horizontal line in orange marks the position of $S_m^2 = 0.1$, which corresponds to the square of four times of the frequency resolution $1/\Delta T$. The circles above the horizontal line corresponds to 78 candidate models in Table 2. The filled circle in the figures corresponds to the best-fitting model (Model 68).

Figure 2(a) presents changes of S_m^2 as a function of the stellar mass M . In the figure, values of M are found to cover a wide range, i.e., $1.67-1.84 M_\odot$, while stellar masses of theoretical models with the same overshooting mixing are found to exhibit good convergence. Therein, values of M converge well to $1.79-1.84 M_\odot$ for models with $f_{\text{ov}} = 0$, to $1.75-1.77 M_\odot$ for models with $f_{\text{ov}} = 0.01$, and to $1.67-1.71 M_\odot$ for models with $f_{\text{ov}} = 0.02$.

Figures 2(b) and 2(c) present changes of S_m^2 as a function of the metallicity Z and the rotation period P_{rot} , respectively. It can be clearly seen in the figures that values of Z converge well to $0.012-0.016$, and those of P_{rot} converge well to $3.6-4.7$ days.

Figure 2(d) presents changes of S_m^2 as a function of the overshooting parameter f_{ov} . As shown in the figure, the best-fitting model has an intermediate overshooting ($f_{\text{ov}} = 0.02$). Besides, we find that theoretical models without overshooting ($f_{\text{ov}} = 0$) and with moderate overshooting ($f_{\text{ov}} = 0.01$) can also reproduce well the eight δ Scuti frequencies.

Figures 3(a)-(d) depict changes of S_m^2 as a function of the effective temperature T_{eff} , the luminosity L , the stellar radial R , and the gravitational acceleration $\log g$, respectively. In Figures 3(a) and 3(b), it can be noticed that both of T_{eff} and L distribute over a wide range, i.e., $T_{\text{eff}} = 7727-8273 \text{ K}$ and $L = 10.051-14.054 L_\odot$. In Figures 3(c) and 3(d), R and $\log g$ distribute over a relatively smaller range, $R = 1.771-1.827 R_\odot$ and $\log g = 4.164-4.179$. Moreover, R and $\log g$ of theoretical models with the same overshooting are found to be in good convergence.

Figure 3(e) depicts changes of S_m^2 as a function of the mass fraction of central hydrogen X_c , and Figure 3(f) depicts changes of S_m^2 as a function of ages of stars. Figure 3(e) shows that X_c distribute between 0.468 and 0.499, and Figure 3(f) shows that their ages range from 0.567 Gyr to 0.891 Gyr. This results indicate that the primary star of CoRoT 100866999 is being in main sequence stage.

Based on the above considerations, fundamental parameters of the primary star derived from the asteroseismic models are listed in Table 3. They match well the parameters obtained from the eclipsing light curve fit given by Chapellier & Mathias (2013). Table 4 lists model frequencies of the best-fitting model. Table 5 lists comparisons between model frequencies of the best-fitting model and the observed δ Scuti frequencies. Based on the comparisons, frequencies p_1 and p_5 are identified as two dipole modes, and p_3 , p_4 , p_6 , and p_7 as four quadrupole modes. In particular, frequencies p_4 and p_7 are identified as two components of one quintuplet.

5. DISCUSSIONS

In Section 4, we have introduced our fitting results. Physical parameters of theoretical models with different overshooting have a certain dispersion, while those of theoretical models with the same overshooting exhibit good convergence. In order to explain this, propagating properties of the oscillation modes in the star are examined in detail.

Figure 4 illustrates the profiles of Brunt–Väisälä frequency N , characteristic acoustic frequencies S_ℓ ($\ell = 1$ and 2) and hydrogen abundance X_H inside the best-fitting model. Figure 5 illustrates the scaled eigenfunctions inside the best-fitting model. The vertical line in Figure 5 denotes the boundary of the convective core ($\nabla_r = \nabla_{\text{ad}}$). The inner zone is the convective core, and the outer zone is the radiation envelope. It can be clearly seen in Figure 5 that the fundamental radial mode F and the radial first overtone mode p_2 propagate mainly in the stellar envelope, and then characterize the features of the stellar envelope. For those nonradial oscillation modes, we find that p_1 is predominantly a g mode with largest amplitude near the edge of the convective core, and the others exhibit a mixed character with substantial amplitudes near the edge of the convective core and the surface. Therefore, the nonradial oscillation modes can give strong constraints on conditions of the convective core.

The acoustic radius τ_0 is the sound travel time between the center and the surface of the star. It is defined by Aerts et al. (2010) as

$$\tau_0 = \int_0^R \frac{dr}{c_s}, \quad (6)$$

where c_s the adiabatic sound speed. In general, the value of c_s in the envelope is much smaller than that in the convective core, thus τ_0 is suitable to characterize features of the stellar envelope. Given that the nonradial modes have substantial amplitudes near the edge of the convective core, we use the relative radius of the convective core R_{conv}/R to characterize features of the deep interior of the star.

To fit the eight δ Scuti frequencies, both the convective core and the stellar envelope of the theoretical model need to be matched to the actual structure of CoRoT 100866999. Figures 6 and 7 show changes of S_m^2 as a function of τ_0 and R_{conv}/R , respectively. In the figures, we find that τ_0 of the candidate models converge well to 7154^{+18}_{-61} s and R_{conv}/R of the candidate models converge well to $0.0931^{+0.0003}_{-0.0013}$. This suggests that they are nearly alike in structure.

The relation between the large frequency separation and the mean density of δ Scuti stars have been investigated in details (e.g., Suárez et al. 2014; García Hernández 2015). García Hernández (2017) updates the relation as

$$\bar{\rho}/\rho_{\odot} = 1.50^{+0.09}_{-0.10} (\Delta\nu/\Delta\nu_{\odot})^{2.04^{+0.04}_{-0.04}}, \quad (7)$$

where $\Delta\nu_{\odot} = 134.8 \mu\text{Hz}$ (Kjeldsen, Bedding & Christensen-Dalsgaard 2008). For the best-fitting model, the mean density $\bar{\rho}_{\text{mod}}$ and the surface gravity $\log g_{\text{mod}}$ are estimated to be 0.422 g/cm^3 and 4.166 , respectively. Besides, we estimate the averaged frequency spacing $(\Delta\nu)_{\text{avg}}$ of p modes in Table 4 to be $59.258 \mu\text{Hz}$ based on the best-fitting model. According to equation (7), $(\Delta\nu)_{\text{avg}}$ corresponds to a mean density of $0.395 \pm 0.038 \text{ g/cm}^3$ and a surface gravity of $4.138^{+0.040}_{-0.044}$, matching well the mean density and surface gravity of the best-fitting model.

The rotation period P_{rot} of the primary star is determined to be $P_{\text{rot}} = 4.1^{+0.6}_{-0.5}$ days, which is slower than the orbital period $P_{\text{orb}} = 2.80889$ days. Ouazzani et al. (2010) investigated the rotational splittings of β Cephei stars, and found that the threshold of validity of perturbative methods is extended to 10% of the break-up velocity. The break-up velocity v_{crit} of the primary star is estimated to be $424 \pm 2 \text{ km s}^{-1}$. The rotation velocity v_e is estimated to be $22 \pm 3 \text{ km s}^{-1}$ according to $v_e = 2\pi R/P_{\text{rot}}$, about 5.2% of the break-up velocity v_{crit} , thus the linear perturbation method is still valid. Moreover, given that its low rotational velocity, the effect of rotation on the stellar structure and evolution are not included in our calculations. According to work of Saio (1981), Dziembowski & Goode (1992), and Aerts et al. (2010), the first-order effect of rotation on pulsation is in proportion to $1/P_{\text{rot}}$, and that of the second-order is in proportion to $1/(P_{\text{rot}}^2 \nu_{\ell,n})$. The ratio of the second-order and the first-order effect of rotation can be estimated to be in the order of $1/(P_{\text{rot}} \nu_{\ell,n})$, where $1/P_{\text{rot}}$ is estimated to be $2.82^{+0.39}_{-0.36} \mu\text{Hz}$ and $\nu_{\ell,n}$ ranges from $188.113 \mu\text{Hz}$ to $308.669 \mu\text{Hz}$. The second-order effect of rotation is much less than that of the first-order one. Hence the second-order effect of rotation on pulsation is not included in this work.

Gizon & Solanki (2003) investigated the relation of amplitude of the nonradial oscillation and the inclination

angle i of the stellar rotation axes in details. The inclination angle i of CoRoT 100866999 is determined to be 80 ± 2 degrees (Chapellier & Mathias 2013). According to work of Gizon & Solanki (2003), dipole modes with $m = \pm 1$ are more visible than those with $m = 0$, and quadrupole modes with $m = 0$ and ± 2 exhibit more visible than those with $m = \pm 1$. As shown in Table 5, amplitudes of p_1, p_3, p_4 , and p_6 meet the predictions, while those of p_5 and p_7 do not conform with the relation. The studies of Gizon & Solanki (2003) is on the basis of the assumption that energy equals each other between modes with different azimuthal number. However, this assumption is not always valid for δ Scuti stars, such as for KIC 9244992 (Saio et al. 2015), the relative amplitudes of modes with $m = 0$ and those with $m = \pm 1$ varies in different multiplets.

Finally, it should be pointed out that all of the above analyses are based on the δ Scuti frequencies. The pulsating primary star is a hybrid δ Sct- γ Dor star with two clearly distinct frequencies domains (Chapellier & Mathias 2013). Except for the independent δ Scuti frequencies, there are 63 independent γ Doradus frequencies. In Table 4, it can be seen that model frequencies in the interval $[3; 60] \mu\text{Hz}$ are very dense, including 94 theoretical frequencies with $\ell = 1$ and 165 theoretical frequencies with $\ell = 2$. According to equation (3), each mode with $\ell = 1$ will split into three different frequencies, and each mode with $\ell = 2$ will split into five different frequencies. Considering the effects of rotation on pulsation, model frequencies will become much denser.

Based on the best-fitting model, we compare model frequencies with the 63 γ Doradus frequencies. The model frequency nearest to observations is regarded as its possible model counterpart, and the comparing results are listed in Table 6. In Table 6, the 22 frequencies with a nearly constant period separation identified by Chapellier & Mathias (2013) are marked in bold-face. It can be seen in Table 6 that these 22 frequencies can be well reproduced based on our best-fitting model, and their period differences between model frequencies of the best-fitting model and observations range from 0 days for f_{38} to 0.0035 days for f_{46} . Deviations from the rigorously uniform period spacing for model frequencies nearly equal to those for the 22 observed modes. Furthermore, we compare the γ Dor frequencies with other stellar models in the grid, due to very dense of the model frequencies, the γ Dor frequencies can also be well reproduced. Therefore, we do not use the γ Doradus frequencies to restrict our theoretical models in this work.

6. SUMMARY AND CONCLUSIONS

We have carried out largely numerical calculations and detailed asteroseismic analyses for the pulsating primary star of CoRoT 100866999. The main results of this work are concluded as follows:

1. The pulsating primary star of CoRoT 100866999 is found to be a main sequence star with a rotation period of $4.1^{+0.6}_{-0.5}$ days. The primary star rotates slower than the orbital motion.

2. Physical parameters of the primary star of CoRoT 100866999 are determined to be $M = 1.71^{+0.13}_{-0.04} M_{\odot}$, $Z = 0.012^{+0.004}_{-0.000}$, $f_{\text{ov}} = 0.02^{+0.00}_{-0.02}$, $T_{\text{eff}} = 8024^{+249}_{-297} \text{ K}$, $L = 11.898^{+2.156}_{-1.847} L_{\odot}$, $\log g = 4.166^{+0.013}_{-0.002}$, $R = 1.787^{+0.040}_{-0.016}$

R_{\odot} , and $X_c = 0.488^{+0.011}_{-0.020}$. The asteroseismic parameters match well those from the eclipsing curve fit given by Chapellier & Mathias (2013).

3. Based on comparisons between model frequencies and observations, p_1 and p_5 are identified as two dipole modes, and p_3 , p_4 , p_6 , and p_7 as four quadrupole modes. Moreover, we find that frequencies p_4 and p_7 are two component of one quintuplet.

4. Based on the best-fitting model, p_1 is found to be a g mode, and the other nonradial modes are found to exhibit distinct mixed characters. These modes provide strong constraints on conditions of the deep interior of the star. Finally, the relative radius of the convective core of CoRoT 100866999 is suggested to be $R_{\text{conv}}/R = 0.0931^{+0.0003}_{-0.0013}$.

The authors thank for the fund from the NSFC of China (Grant No. 11333006, 11521303, 11833002, 11803082). Xinghao Chen appreciate the support the West Light Foundation of The Chinese Academy of Sciences. The authors gratefully acknowledge the computing time granted by the Yunnan Observatories, and provided on the facilities at the Yunnan Observatories Supercomputing Platform. The authors are sincerely grateful to an anonymous referee for instructive advice and productive suggestions. Xinghao Chen is also thankful for fruitful discussions with Jianheng Guo, Jie Su, and Tao Wu.

APPENDIX

INLIST FILE OF PULSEADIPLS IN MESA (VERSION 10398)

```
! inlist_pulse
&star_job
  astero_just_call_my_extras_check_model = .true.
  create_pre_main_sequence_model = .true.
  change_lnPgas_flag = .true.
  new_lnPgas_flag = .true.
  change_initial_net = .true.
  new_net_name = 'o18_and_ne22.net'
  kappa_file_prefix = 'a09'
  kappa_lowT_prefix = 'lowT_fa05_a09p'
  initial_zfracs = 6
  relax_to_this_tau_factor = 1.5d-3
  relax_tau_factor = .true.
/ ! end of star_job namelist
&controls
  initial_mass = 1.71
  initial_z = 0.012
  initial_y = 0.26496
  overshoot_f_above_burn_h_core = 0.020

  min_overshoot_q = 1d-3
  D_mix_ov_limit = 1d-2
  overshoot_f0_above_burn_h_core = 0.005
  MLT_option = 'ML1'
  mixing_length_alpha = 1.90
  calculate_Brunt_N2 = .true.
  use_brunt_gradmuX_form = .true.
  which_atm_option = 'simple_photosphere' !default

  history_interval = 1
  max_num_profile_models = 80000
  xa_central_lower_limit_species(1) = 'h1'
  xa_central_lower_limit(1) = 5d-5

  use_other_mesh_functions= .true.
  mesh_delta_coeff = 0.90
  M_function_weight = 50
  max_center_cell_dq = 1d-10
  varcontrol_target = 5d-5 !for main-sequence models (2d-4 for pre-main sequence models)
  max_years_for_timestep = 1d6
/ ! end of controls namelist
```

REFERENCES

Aerts, C., Christensen-Dalsgaard, J., & Kurtz, D. W. 2010,
 Asteroseismology, Astronomy and Astrophysics Library (Berlin:
 Springer)

Asplund, M., Grevesse, N., Sauval, A. J., & Scott, P. 2009,
 ARA&A, 47, 481

TABLE 1

EIGHT INDEPENDENT δ SCUTI FREQUENCIES OBTAINED BY CHAPELLIER & MATHIAS (2013). ID REPRESENTS THE SERIAL NUMBER OF THE OBSERVED FREQUENCIES IN CHAPELLIER & MATHIAS (2013). FREQ. REPRESENTS THE OBSERVED FREQUENCY. AMPL. REPRESENTS THE AMPLITUDES IN UNIT OF MMAG. S/N REPRESENTS THE SIGNAL-TO-NOISE RATIO.

ID	Freq. (d^{-1})	Freq. (μ Hz)	Ampl. (mmag)	S/N
<i>F</i>	16.9803	196.531	11.623	515.5
<i>p</i> ₁	16.2530	188.113	0.508	22.8
<i>p</i> ₂	21.8711	253.138	0.449	23.3
<i>p</i> ₃	17.5521	203.149	0.223	10.1
<i>p</i> ₄	21.6053	250.061	0.167	8.5
<i>p</i> ₅	17.5674	203.326	0.151	6.8
<i>p</i> ₆	26.6690	308.669	0.126	6.6
<i>p</i> ₇	21.8441	252.825	0.125	6.5

Baglin, A., Auvergne, M., Barge, P., et al. 2006, in ESA SP 1306, The CoRoT Mission Pre-Launch StatusStellar Seismology and Planet Finding, ed. M. Fridlund et al. (Paris: ESA), 33

Baker, N., & Kippenhahn, R. 1962, *Z. f. Astrophys.*, 54, 114

Baker, N., & Kippenhahn, R. 1965, *APJ*, 142, 868

Balona, L. A. 2011, *MNRAS*, 415, 1691

Balona, L. A., Daszyńska-Daszkiewicz, J., & Pamyatnykh, A. A. 2015, *MNRAS*, 452, 3073

Barceló Forteza, S., Michel, E., Roca Cortés, T., & García, R. A. 2015, *A&A*, 579, A133

Barceló Forteza, S., Roca Cortés, T., & García, R. A. 2018, *A&A*, 614, A46

Breger, M. 2000, *Delta Scuti and Related Stars*, 210, 3

Böhm-Vitense, E. 1958, *ZAp*, 46, 108

Borucki, W. J., Koch, D., Basri, G., et al. 2010, *Science*, 327, 977

Bowman, D. M., & Kurtz, D. W. 2014, *MNRAS*, 444, 1909

Bowman, D. M., Kurtz, D. W., Breger, M., Murphy, S. J., & Holdsworth, D. L. 2016, *MNRAS*, 460, 1970

Campbell, W. W., & Wright, W. H. 1900, *ApJ*, 12,

Chapellier, E., Mathias, P., Weiss, W. W., Le Contel, D., & Debosscher, J. 2012, *A&A*, 540, A117

Chapellier, E., & Mathias, P. 2013, *A&A*, 556, A87

Chen, X. H., & Li, Y. 2018, *ApJ*, 866, 147

Chen, X. H., & Li, Y. 2019, *ApJ*, 872, 156

Chevalier, C. 1971, *A&A*, 14, 24

Christensen-Dalsgaard, J. 2008, *Ap&SS*, 316, 113

Dupret, M.-A., Grigahcène, A., Garrido, R., Gabriel, M., & Scuflaire, R. 2004, *A&A*, 414, L17

Dupret, M.-A., Grigahcène, A., Garrido, R., Gabriel, M., & Scuflaire, R. 2005, *A&A*, 435, 927

Dziembowski, W. A., & Goode, P. R. 1992, *ApJ*, 394, 670

Ferguson, J. W., Alexander, D. R., Allard, F., et al. 2005, *ApJ*, 623, 585

Fitch, W. S. 1981, *ApJ*, 249, 218

Freytag, B., Ludwig, H.-G., & Steffen, M. 1996, *A&A*, 313, 497

García Hernández, A., Martín-Ruiz, S., Monteiro, M. J. P. F. G., et al. 2015, *ApJ*, 811, L29

García Hernández, A., Suárez, J. C., Moya, A., et al. 2017, *MNRAS*, 471, L140

Grigahcène, A., Dupret, M.-A., Gabriel, M., Garrido, R., & Scuflaire, R. 2005, *A&A*, 434, 1055

Grigahcène, A., Antoci, V., Balona, L., et al. 2010, *ApJ*, 713, L192

Guzik, J. A., Kaye, A. B., Bradley, P. A., Cox, A. N., & Neuforge, C. 2000, *ApJ*, 542, L57

Gizon, L., & Solanki, S. K. 2003, *ApJ*, 589, 1009

Henry, G. W., & Fekel, F. C. 2005, *AJ*, 129, 2026

Henry, G. W., Fekel, F. C., & Henry, S. M. 2011, *AJ*, 142, 39

Herwig, F. 2000, *A&A*, 360, 952

Iglesias, C. A., & Rogers, F. J. 1996, *ApJ*, 464, 943

Kurtz, D. W., Saio, H., Takata, M., et al. 2014, *MNRAS*, 444, 102

Kaye, A. B., Handler, G., Krisciunas, K., Poretti, E., & Zerbi, F. M. 1999, *PASP*, 111, 840

Kjeldsen, H., Bedding, T. R., & Christensen-Dalsgaard, J. 2008, *ApJ*, 683, L175

Li, T. D., Bedding, T. R., Huber, D., et al. 2018, *MNRAS*, 475, 981

Li, Y., & Stix, M. 1994, *A&A*, 286, 815

Miglio, A., Montalbán, J., Noels, A., & Eggenberger, P. 2008, *MNRAS*, 386, 1487

Moya, A., Suárez, J. C., García Hernández, A., & Mendoza, M. A. 2017, *MNRAS*, 471, 2491

Ouazzani, R. M., Goupil, M. J., Dupret, M. A., & Reese, D. 2010, *Ap&SS*, 328, 285

Paparó, M., Bognár, Z., Benkő, J. M., et al. 2013, *A&A*, 557, A27

Paparó, M., Benkő, J. M., Hareter, M., & Guzik, J. A. 2016, *ApJS*, 224, 41

Paxton, B., Bildsten, L., Dotter, A., et al. 2011, *ApJS*, 192, 3

Paxton, B., Cantiello, M., Arras, P., et al. 2013, *ApJS*, 208, 4

Paxton, B., Marchant, P., Schwab, J., et al. 2015, *ApJS*, 220, 15

Paxton, B., Schwab, J., Bauer, E. B., et al. 2018, *ApJS*, 234, 34

Poretti, E., Suárez, J. C., Niarchos, P. G., et al. 2005, *A&A*, 440, 1097

Rogers, F. J., & Nayfonov, A. 2002, *ApJ*, 576, 1064

Saio, H. 1981, *ApJ*, 244, 299

Saio, H., Kurtz, D. W., Takata, M., et al. 2015, *MNRAS*, 447, 3264

Sánchez Arias, J. P., Córscico, A. H., & Althaus, L. G. 2017, *A&A*, 597, A29

Suárez, J. C., Garrido, R., & Goupil, M. J. 2006, *A&A*, 447, 649

Suárez, J. C., García Hernández, A., Moya, A., et al. 2014, *A&A*, 563, A7

Sarro, L. M., Debosscher, J., Neiner, C., et al. 2013, *A&A*, 550, A120

Templer, M., Basu, S., & Demarque, P. 2002, *ApJ*, 576, 963

Uytterhoeven, K., Moya, A., Grigahcène, A., et al. 2011, *A&A*, 534, A125

Van Reeth, T., Tkachenko, A., Aerts, C., et al. 2015, *A&A*, 574, A17

Van Reeth, T., Tkachenko, A., & Aerts, C. 2016, *A&A*, 593, A120

Van Reeth, T., Mombarg, J. S. G., Mathis, S., et al. 2018, *A&A*, 618, A24

Walker, G., Matthews, J., Kuschnig, R., et al. 2003, *PASP*, 115, 1023

Xiong, D. R., Deng, L., Zhang, C., & Wang, K. 2016, *MNRAS*, 457, 3163

Zhevakin, S. A. 1963, *Ann. Rev. Astr. Astrophys.*, 1, 367

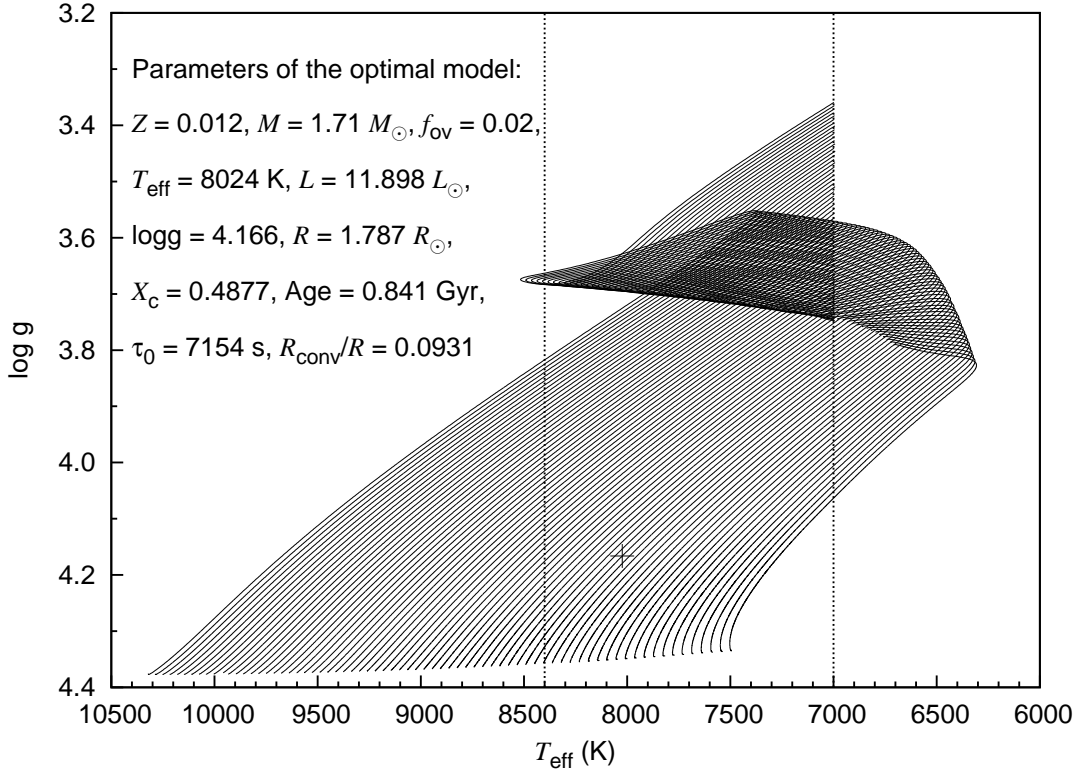


FIG. 1.— Evolutionary tracks of stars with $Z = 0.012$, $f_{\text{ov}} = 0.02$, and M ranging from 1.50 to $2.20 M_{\odot}$ in a step of $0.01 M_{\odot}$. The two dotted lines mark the constraints $7000 \text{ K} < T_{\text{eff}} < 8400 \text{ K}$. The crossing denotes the best-fitting model, whose fundamental parameters are labelled in the top of the figure.

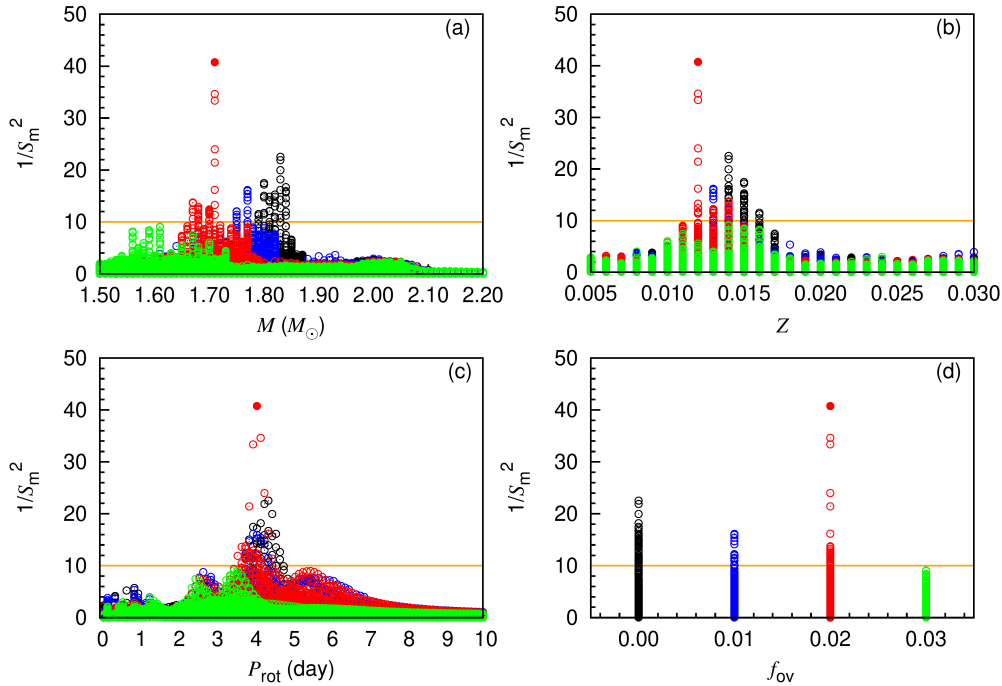


FIG. 2.— Visualisation of fitting results $1/S_m^2$ versus adjustable parameters: stellar mass M , the initial metallicity Z , the rotation period P_{rot} , and the overshooting parameter f_{ov} , respectively. The circles in black, blue, red, and green corresponds to stellar models with $f_{\text{ov}} = 0, 0.01, 0.02$, and 0.03 , respectively. The horizontal line in orange mark the position of $S_m^2 = 0.1$.

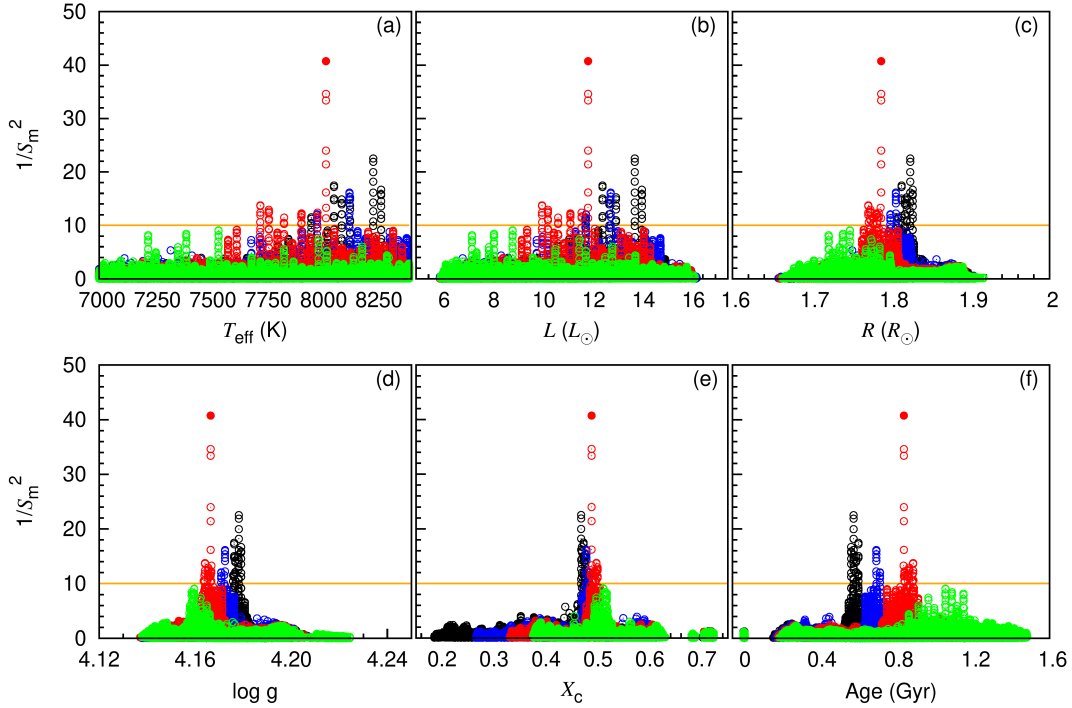


FIG. 3.— Visualisation of fitting results $1/S_m^2$ versus stellar fundamental parameters: the effective temperature T_{eff} , the luminosity L , stellar radius R , the gravitational acceleration $\log g$, the mass fraction of central hydrogen X_c , and the age of stars, respectively. The circles in black, blue, red, and green corresponds to stellar models with $f_{\text{ov}} = 0, 0.01, 0.02$, and 0.03 , respectively. The horizontal line in orange mark the position of $S_m^2 = 0.1$.

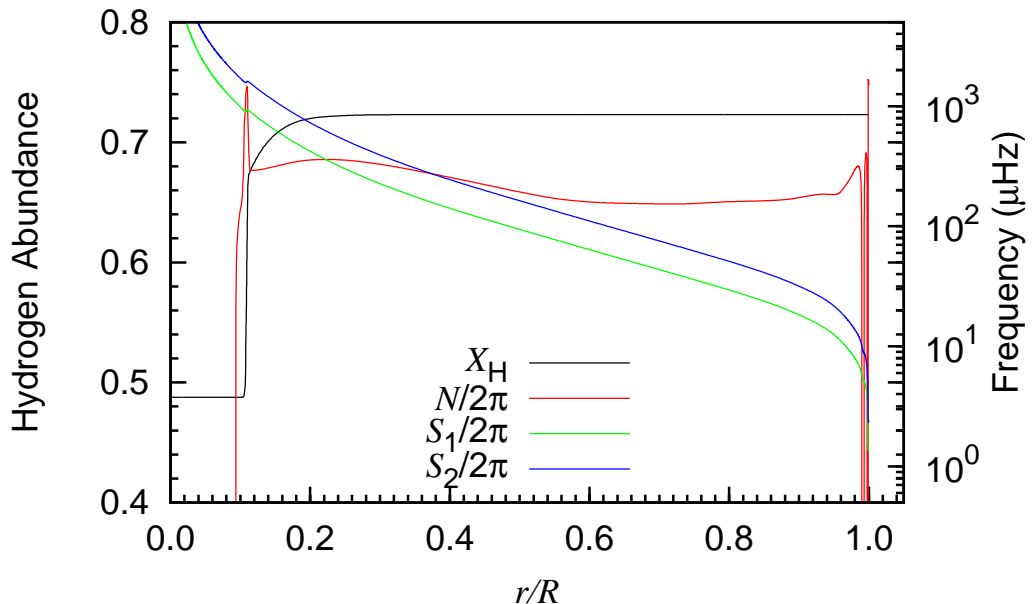


FIG. 4.— Brunt–Väisälä frequency N , characteristic acoustic frequencies S_ℓ ($\ell = 1$ and 2), and hydrogen abundance X_H inside the best-fitting model of CoRoT 100866999.

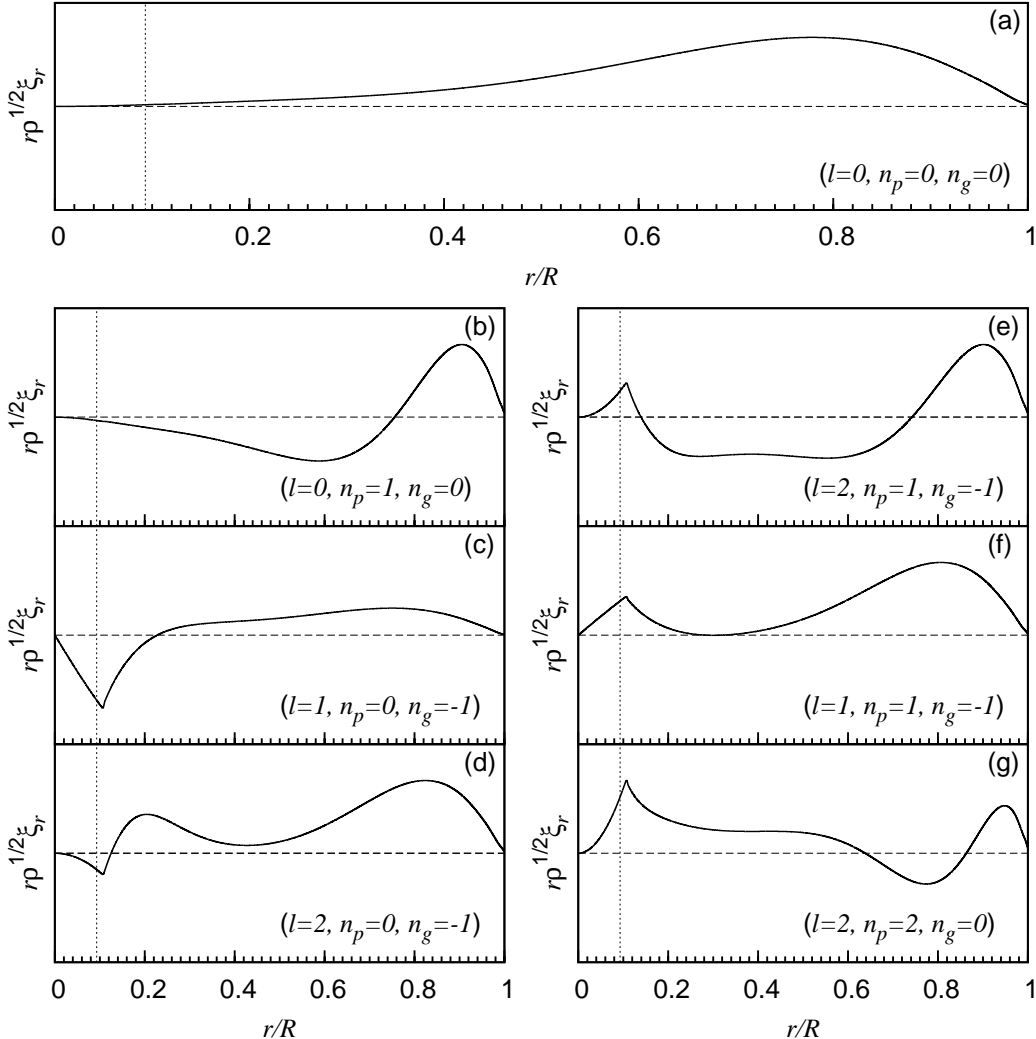


FIG. 5.— Scaled radial displacement eigenfunctions for theoretical modes corresponding to the observed frequencies inside the best-fitting model. Panel (a) corresponds to the fundamental radial mode F . Panel (b) corresponds to the radial first overtone mode p_2 . Panels (c), (d), (f), and (g) correspond to the observed frequencies p_1 , p_3 , p_5 , and p_6 , respectively. Panel (e) corresponds to the observed frequencies p_4 and p_7 . Vertical line marks the boundary of the convective core ($\nabla_r = \nabla_{\text{ad}}$).

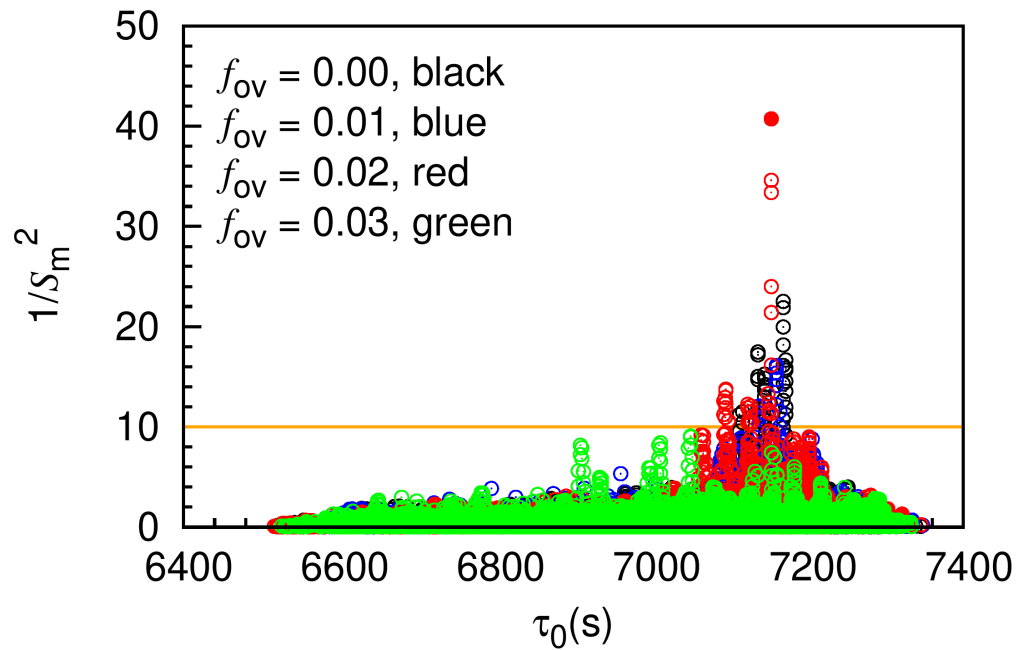


FIG. 6.— Visualisation of fitting results $1/S_m^2$ versus the acoustic radius τ_0 . The circles in black, blue, red, and green corresponds to stellar models with $f_{ov} = 0, 0.01, 0.02$, and 0.03 , respectively. The horizontal line in orange mark the position of $S_m^2 = 0.1$.

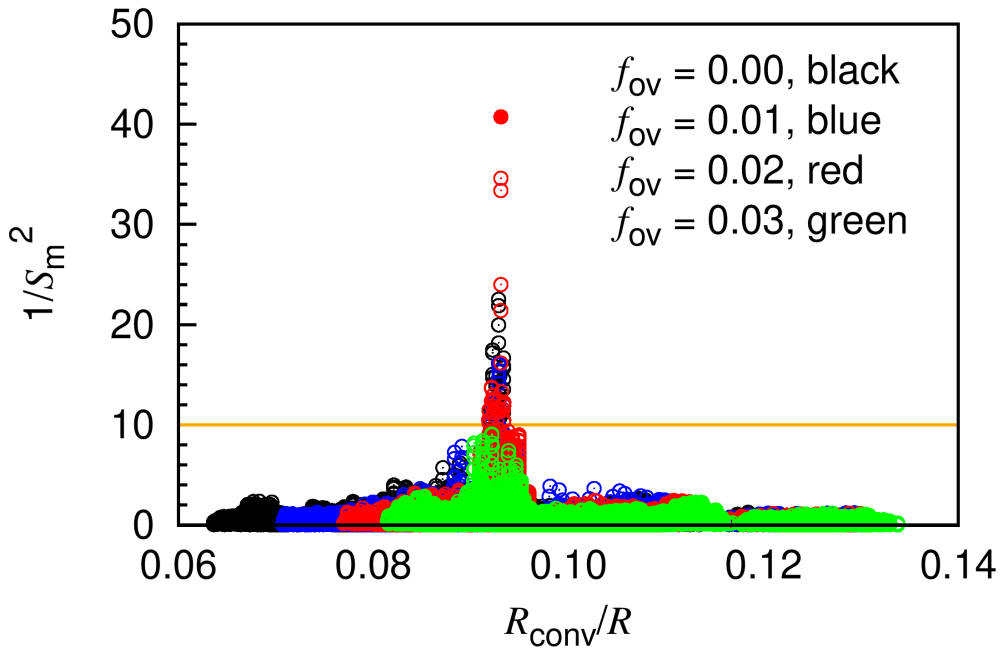


FIG. 7.— Visualisation of fitting results $1/S_m^2$ versus the relative radius of the convective core R_{conv}/R . The circles in black, blue, red, and green corresponds to stellar models with $f_{\text{ov}} = 0, 0.01, 0.02$, and 0.03 , respectively. The horizontal line in orange mark the position of $S_m^2 = 0.1$.

TABLE 2

CANDIDATE MODELS WITH $S_m^2 < 0.10$. THE FIRST COLUMN IS THE SERIAL NUMBER OF CANDIDATE MODELS. P_{rot} IS THE ROTATION PERIOD OF THE STAR. τ_0 IS THE ACOUSTIC RADIUS DEFINED AS EQUATION (6). R_{conv}/R IS THE RELATIVE RADIUS OF THE CONVECTIVE CORE IN THE STAR. X_c IS THE MASS FRACTION OF HYDROGEN IN THE CENTER OF THE STAR.

Model	P_{rot} (day)	Z	M (M_{\odot})	f_{ov}	T_{eff} (K)	L (L_{\odot})	$\log g$ (dex)	R (R_{\odot})	τ_0 (s)	R_{conv}/R (1d-2)	X_c	Age (Gyr)	S_m^2
1	3.80	0.015	1.80	0.00	8061	12.472	4.176	1.813	7137	9.224	0.4723	0.605	0.0875
2	3.80	0.016	1.79	0.00	7959	11.788	4.176	1.809	7113	9.200	0.4806	0.604	0.0890
3	3.90	0.015	1.80	0.00	8061	12.472	4.176	1.813	7137	9.224	0.4723	0.605	0.0665
4	3.90	0.015	1.82	0.00	8133	13.015	4.178	1.820	7145	9.297	0.4758	0.580	0.0910
5	3.90	0.016	1.79	0.00	7957	11.791	4.176	1.809	7117	9.196	0.4802	0.605	0.0868
6	4.00	0.014	1.83	0.00	8238	13.767	4.178	1.824	7169	9.284	0.4677	0.580	0.0930
7	4.00	0.015	1.80	0.00	8061	12.472	4.176	1.813	7136	9.224	0.4723	0.605	0.0572
8	4.00	0.015	1.82	0.00	8133	13.015	4.178	1.820	7145	9.297	0.4758	0.580	0.0730
9	4.00	0.016	1.79	0.00	7957	11.791	4.176	1.809	7117	9.196	0.4802	0.605	0.0957
10	4.10	0.014	1.83	0.00	8238	13.767	4.178	1.824	7169	9.284	0.4677	0.580	0.0699
11	4.10	0.014	1.84	0.00	8273	14.054	4.179	1.827	7172	9.333	0.4691	0.568	0.0836
12	4.10	0.015	1.80	0.00	8061	12.472	4.176	1.813	7137	9.224	0.4723	0.605	0.0582
13	4.10	0.015	1.81	0.00	8095	12.746	4.177	1.817	7146	9.255	0.4734	0.594	0.0826
14	4.10	0.015	1.82	0.00	8133	13.015	4.178	1.820	7145	9.297	0.4758	0.580	0.0655
15	4.20	0.014	1.83	0.00	8238	13.767	4.178	1.824	7169	9.284	0.4677	0.580	0.0550
16	4.20	0.014	1.84	0.00	8273	14.054	4.179	1.827	7172	9.333	0.4691	0.568	0.0687
17	4.20	0.015	1.80	0.00	8061	12.472	4.176	1.813	7134	9.224	0.4723	0.605	0.0679
18	4.20	0.015	1.81	0.00	8095	12.746	4.177	1.817	7146	9.255	0.4734	0.594	0.0705
19	4.20	0.015	1.82	0.00	8133	13.015	4.178	1.820	7145	9.297	0.4758	0.580	0.0673
20	4.30	0.014	1.83	0.00	8238	13.767	4.178	1.824	7169	9.284	0.4677	0.580	0.0457
21	4.30	0.014	1.84	0.00	8273	14.054	4.179	1.827	7172	9.333	0.4691	0.568	0.0629
22	4.30	0.015	1.80	0.00	8061	12.472	4.176	1.813	7137	9.224	0.4723	0.605	0.0852
23	4.30	0.015	1.81	0.00	8095	12.746	4.177	1.817	7146	9.255	0.4734	0.594	0.0673
24	4.30	0.015	1.82	0.00	8133	13.015	4.178	1.820	7145	9.297	0.4758	0.580	0.0770
25	4.40	0.014	1.83	0.00	8238	13.767	4.178	1.824	7169	9.284	0.4677	0.580	0.0444
26	4.40	0.014	1.84	0.00	8273	14.054	4.179	1.827	7172	9.333	0.4691	0.568	0.0599
27	4.40	0.015	1.81	0.00	8095	12.746	4.177	1.817	7146	9.255	0.4734	0.594	0.0718
28	4.40	0.015	1.82	0.00	8133	13.015	4.178	1.820	7145	9.297	0.4758	0.580	0.0935
29	4.50	0.014	1.83	0.00	8238	13.767	4.178	1.824	7169	9.284	0.4677	0.580	0.0501
30	4.50	0.014	1.84	0.00	8273	14.054	4.179	1.827	7172	9.333	0.4691	0.568	0.0638
31	4.50	0.015	1.81	0.00	8095	12.746	4.177	1.817	7146	9.255	0.4734	0.594	0.0831
32	4.60	0.014	1.83	0.00	8238	13.767	4.178	1.824	7169	9.284	0.4677	0.580	0.0620
33	4.60	0.014	1.84	0.00	8273	14.054	4.179	1.827	7172	9.333	0.4691	0.568	0.0738
34	4.70	0.014	1.83	0.00	8238	13.767	4.178	1.824	7169	9.284	0.4677	0.580	0.0791
35	4.70	0.014	1.84	0.00	8273	14.054	4.179	1.827	7172	9.333	0.4691	0.568	0.0891
36	3.80	0.013	1.77	0.01	8130	12.802	4.172	1.806	7160	9.288	0.4779	0.698	0.0817
37	3.90	0.013	1.77	0.01	8130	12.802	4.172	1.806	7160	9.288	0.4779	0.698	0.0680
38	3.90	0.014	1.75	0.01	7984	11.814	4.171	1.799	7138	9.223	0.4828	0.717	0.0910
39	4.00	0.013	1.77	0.01	8130	12.802	4.172	1.806	7160	9.288	0.4779	0.698	0.0619
40	4.00	0.014	1.75	0.01	7984	11.814	4.171	1.799	7138	9.223	0.4828	0.717	0.0836
41	4.10	0.013	1.77	0.01	8130	12.802	4.172	1.806	7160	9.288	0.4779	0.698	0.0627
42	4.10	0.014	1.75	0.01	7984	11.814	4.171	1.799	7138	9.223	0.4828	0.717	0.0829
43	4.20	0.013	1.77	0.01	8130	12.802	4.172	1.806	7160	9.288	0.4779	0.698	0.0650
44	4.20	0.014	1.75	0.01	7984	11.814	4.171	1.799	7138	9.223	0.4828	0.717	0.0879
45	4.30	0.013	1.77	0.01	8130	12.802	4.172	1.806	7160	9.288	0.4779	0.698	0.0708
46	4.30	0.014	1.75	0.01	7984	11.814	4.171	1.799	7138	9.223	0.4828	0.717	0.0978
47	4.40	0.013	1.77	0.01	8129	12.806	4.172	1.807	7165	9.283	0.4774	0.699	0.0867
48	4.50	0.013	1.77	0.01	8129	12.806	4.172	1.807	7165	9.283	0.4774	0.699	0.0999
49	3.60	0.014	1.67	0.02	7728	10.051	4.164	1.771	7095	9.213	0.4971	0.890	0.0840
50	3.70	0.013	1.70	0.02	7914	11.185	4.167	1.782	7124	9.337	0.4945	0.845	0.0955
51	3.70	0.014	1.67	0.02	7728	10.051	4.164	1.771	7095	9.213	0.4971	0.890	0.0734
52	3.80	0.012	1.70	0.02	7986	11.633	4.165	1.784	7150	9.283	0.4861	0.860	0.0857
53	3.80	0.012	1.71	0.02	8025	11.894	4.167	1.787	7149	9.313	0.4880	0.840	0.0753
54	3.80	0.013	1.70	0.02	7914	11.185	4.167	1.782	7124	9.337	0.4945	0.845	0.0840
55	3.80	0.014	1.67	0.02	7728	10.051	4.164	1.771	7095	9.213	0.4971	0.890	0.0728
56	3.80	0.014	1.68	0.02	7767	10.282	4.166	1.773	7093	9.233	0.4994	0.868	0.0890
57	3.90	0.012	1.70	0.02	7986	11.633	4.165	1.784	7150	9.283	0.4861	0.860	0.0807
58	3.90	0.012	1.71	0.02	8024	11.898	4.166	1.787	7154	9.309	0.4877	0.841	0.0467
59	3.90	0.013	1.70	0.02	7914	11.185	4.167	1.782	7124	9.337	0.4945	0.845	0.0816
60	3.90	0.014	1.67	0.02	7728	10.051	4.164	1.771	7095	9.213	0.4971	0.890	0.0806
61	3.90	0.014	1.68	0.02	7767	10.282	4.166	1.773	7093	9.233	0.4994	0.868	0.0794
62	4.00	0.012	1.70	0.02	7986	11.633	4.165	1.784	7150	9.283	0.4861	0.860	0.0876
63	4.00	0.012	1.71	0.02	8024	11.898	4.166	1.787	7154	9.309	0.4877	0.841	0.0300
64	4.00	0.013	1.68	0.02	7835	10.692	4.164	1.777	7126	9.186	0.4902	0.886	0.0974
65	4.00	0.013	1.70	0.02	7913	11.189	4.166	1.782	7127	9.334	0.4942	0.846	0.0828
66	4.00	0.014	1.67	0.02	7727	10.054	4.164	1.772	7099	9.209	0.4968	0.891	0.0944
67	4.00	0.014	1.68	0.02	7766	10.285	4.165	1.774	7095	9.229	0.4990	0.869	0.0774
68	4.10	0.012	1.71	0.02	8024	11.898	4.166	1.787	7154	9.309	0.4877	0.841	0.0246
69	4.10	0.013	1.68	0.02	7835	10.692	4.164	1.777	7126	9.186	0.4902	0.886	0.0872
70	4.10	0.013	1.70	0.02	7913	11.189	4.166	1.782	7127	9.334	0.4942	0.846	0.0869
71	4.10	0.014	1.68	0.02	7766	10.285	4.165	1.774	7095	9.229	0.4990	0.869	0.0810
72	4.20	0.012	1.71	0.02	8024	11.898	4.166	1.787	7154	9.309	0.4877	0.841	0.0289
73	4.20	0.013	1.68	0.02	7834	10.695	4.164	1.778	7129	9.182	0.4899	0.887	0.0952
74	4.20	0.013	1.70	0.02	7913	11.189	4.166	1.782	7127	9.334	0.4942	0.846	0.0971
75	4.20	0.014	1.68	0.02	7766	10.285	4.165	1.774	7095	9.229	0.4990	0.869	0.0913
76	4.30	0.012	1.71	0.02	8								

TABLE 3

FUNDAMENTAL PARAMETERS OF THE PRIMARY STAR OF CoRoT 100866999. P_{rot} REPRESENTS THE ROTATION PERIOD OF THE STAR. τ_0 REPRESENTS THE ACOUSTIC RADIUS DEFINED AS EQUATION (6). R_{conv}/R IS THE RELATIVE RADIUS OF THE CONVECTIVE CORE IN THE STAR. X_c REPRESENTS THE MASS FRACTION OF HYDROGEN IN THE CENTER OF THE STAR.

Parameter	Values
$M(M_\odot)$	$1.67 - 1.84 (1.71^{+0.13}_{-0.04})$
Z	$0.012 - 0.016 (0.012^{+0.004}_{-0.000})$
f_{ov}	$0 - 0.02 (0.02^{+0.00}_{-0.02})$
$P_{\text{rot}}(\text{day})$	$3.6 - 4.7 (4.1^{+0.6}_{-0.5})$
$T_{\text{eff}} (\text{K})$	$7727 - 8273 (8024^{+249}_{-297})$
$\log g (\text{dex})$	$4.164 - 4.179 (4.166^{+0.013}_{-0.002})$
$R (R_\odot)$	$1.771 - 1.827 (1.787^{+0.040}_{-0.016})$
$L (L_\odot)$	$10.051 - 14.054 (11.898^{+2.156}_{-1.847})$
X_c	$0.468 - 0.499 (0.488^{+0.011}_{-0.020})$
Age (Gyr)	$0.567 - 0.891 (0.841^{+0.050}_{-0.274})$
$\tau_0 (\text{s})$	$7093 - 7172 (7154^{+18}_{-61})$
R_{conv}/R	$0.0918 - 0.0934 (0.0931^{+0.0003}_{-0.0013})$

TABLE 4

THEORETICAL MODEL FREQUENCIES OF THE BEST-FITTING MODEL. ν_{mod} IS THE MODEL FREQUENCIES IN UNIT OF μHz , ℓ IS THE SPHERICAL HARMONIC DEGREE, n_p AND n_g ARE THE NUMBER OF RADIAL ORDERS IN P-MODE PROPAGATION CAVITY AND G-MODE PROPAGATION CAVITY, RESPECTIVELY. $\beta_{\ell,n}$ IS THE ROTATIONAL PARAMETERS DEFINED AS EQUATION (3).

ν_{mod}	(ℓ, n_p, n_g)	$\beta_{\ell,n}$									
196.2583	(0,0, 0)	0.503	9.0610	(1,0, -32)	0.504	3.7467	(2,0, -137)	0.834	7.6076	(2,0, -67)	0.834
253.3330	(0,1, 0)	0.503	9.3495	(1,0, -31)	0.504	3.7740	(2,0, -136)	0.834	7.7188	(2,0, -66)	0.834
311.0961	(0,2, 0)	0.503	9.6595	(1,0, -30)	0.504	3.8019	(2,0, -135)	0.834	7.8321	(2,0, -65)	0.834
368.6966	(0,3, 0)	0.503	9.9826	(1,0, -29)	0.504	3.8306	(2,0, -134)	0.834	7.9490	(2,0, -64)	0.834
			10.3010	(1,0, -28)	0.504	3.8598	(2,0, -133)	0.834	8.0712	(2,0, -63)	0.834
3.0217	(1,0, -98)	0.500	10.6122	(1,0, -27)	0.505	3.8895	(2,0, -132)	0.834	8.1994	(2,0, -62)	0.834
3.0525	(1,0, -97)	0.500	10.9678	(1,0, -26)	0.505	3.9193	(2,0, -131)	0.834	8.3331	(2,0, -61)	0.834
3.0840	(1,0, -96)	0.500	11.3892	(1,0, -25)	0.505	3.9492	(2,0, -130)	0.834	8.4716	(2,0, -60)	0.834
3.1164	(1,0, -95)	0.500	11.8657	(1,0, -24)	0.505	3.9793	(2,0, -129)	0.834	8.6147	(2,0, -59)	0.834
3.1498	(1,0, -94)	0.500	12.3912	(1,0, -23)	0.506	4.0100	(2,0, -128)	0.834	8.7615	(2,0, -58)	0.834
3.1840	(1,0, -93)	0.500	12.9617	(1,0, -22)	0.506	4.0414	(2,0, -127)	0.834	8.9119	(2,0, -57)	0.835
3.2188	(1,0, -92)	0.500	13.5628	(1,0, -21)	0.506	4.0736	(2,0, -126)	0.834	9.0671	(2,0, -56)	0.835
3.2542	(1,0, -91)	0.500	14.1473	(1,0, -20)	0.506	4.1065	(2,0, -125)	0.834	9.2289	(2,0, -55)	0.835
3.2899	(1,0, -90)	0.501	14.7116	(1,0, -19)	0.507	4.1400	(2,0, -124)	0.834	9.3980	(2,0, -54)	0.835
3.3263	(1,0, -89)	0.501	15.4063	(1,0, -18)	0.507	4.1738	(2,0, -123)	0.834	9.5742	(2,0, -53)	0.835
3.3635	(1,0, -88)	0.501	16.2674	(1,0, -17)	0.508	4.2078	(2,0, -122)	0.834	9.7576	(2,0, -52)	0.835
3.4017	(1,0, -87)	0.501	17.2756	(1,0, -16)	0.509	4.2420	(2,0, -121)	0.834	9.9474	(2,0, -51)	0.835
3.4412	(1,0, -86)	0.501	18.4364	(1,0, -15)	0.510	4.2766	(2,0, -120)	0.834	10.1442	(2,0, -50)	0.835
3.4819	(1,0, -85)	0.501	19.7688	(1,0, -14)	0.511	4.3119	(2,0, -119)	0.834	10.3493	(2,0, -49)	0.835
3.5236	(1,0, -84)	0.501	21.2921	(1,0, -13)	0.512	4.3483	(2,0, -118)	0.834	10.5637	(2,0, -48)	0.835
3.5659	(1,0, -83)	0.501	22.9950	(1,0, -12)	0.512	4.3856	(2,0, -117)	0.834	10.7871	(2,0, -47)	0.835
3.6084	(1,0, -82)	0.501	24.7207	(1,0, -11)	0.511	4.4237	(2,0, -116)	0.834	11.0194	(2,0, -46)	0.835
3.6514	(1,0, -81)	0.501	26.4240	(1,0, -10)	0.512	4.4622	(2,0, -115)	0.834	11.2604	(2,0, -45)	0.835
3.6955	(1,0, -80)	0.501	28.8158	(1,0, -9)	0.515	4.5013	(2,0, -114)	0.834	11.5103	(2,0, -44)	0.835
3.7412	(1,0, -79)	0.501	32.1554	(1,0, -8)	0.517	4.5407	(2,0, -113)	0.834	11.7706	(2,0, -43)	0.835
3.7887	(1,0, -78)	0.501	36.6016	(1,0, -7)	0.518	4.5806	(2,0, -112)	0.834	12.0435	(2,0, -42)	0.835
3.8377	(1,0, -77)	0.501	42.5975	(1,0, -6)	0.519	4.6214	(2,0, -111)	0.834	12.3321	(2,0, -41)	0.835
3.8879	(1,0, -76)	0.501	50.9201	(1,0, -5)	0.519	4.6632	(2,0, -110)	0.834	12.6393	(2,0, -40)	0.836
3.9389	(1,0, -75)	0.501	63.0243	(1,0, -4)	0.515	4.7059	(2,0, -109)	0.834	12.9664	(2,0, -39)	0.836
3.9904	(1,0, -74)	0.501	82.1270	(1,0, -3)	0.503	4.7496	(2,0, -108)	0.834	13.3124	(2,0, -38)	0.836
4.0425	(1,0, -73)	0.501	116.5050	(1,0, -2)	0.485	4.7941	(2,0, -107)	0.834	13.6739	(2,0, -37)	0.836
4.0959	(1,0, -72)	0.501	189.9109	(1,0, -1)	0.565	4.8391	(2,0, -106)	0.834	14.0445	(2,0, -36)	0.836
4.1514	(1,0, -71)	0.501	203.3093	(1,1, -1)	0.898	4.8757	(2,0, -105)	0.835	14.4167	(2,0, -35)	0.836
4.2092	(1,0, -70)	0.501	262.1546	(1,1, 0)	0.994	4.8847	(2,0, -104)	0.834	14.7956	(2,0, -34)	0.836
4.2692	(1,0, -69)	0.501	325.5027	(1,2, 0)	0.996	4.9313	(2,0, -103)	0.834	15.2053	(2,0, -33)	0.836
4.3311	(1,0, -68)	0.501	389.7996	(1,3, 0)	0.994	4.9788	(2,0, -102)	0.834	15.6602	(2,0, -32)	0.837
4.3944	(1,0, -67)	0.501			5.0273	(2,0, -101)	0.834	16.1576	(2,0, -31)	0.837	
4.4588	(1,0, -66)	0.501	3.0020	(2,0, -171)	0.833	5.0771	(2,0, -100)	0.834	16.6881	(2,0, -30)	0.837
4.5243	(1,0, -65)	0.501	3.0195	(2,0, -170)	0.833	5.1281	(2,0, -99)	0.834	17.2333	(2,0, -29)	0.837
4.5917	(1,0, -64)	0.501	3.0373	(2,0, -169)	0.833	5.1799	(2,0, -98)	0.834	17.7636	(2,0, -28)	0.837
4.6623	(1,0, -63)	0.501	3.0555	(2,0, -168)	0.833	5.2325	(2,0, -97)	0.834	18.3035	(2,0, -27)	0.838
4.7363	(1,0, -62)	0.501	3.0740	(2,0, -167)	0.833	5.2859	(2,0, -96)	0.834	18.9366	(2,0, -26)	0.838
4.8135	(1,0, -61)	0.501	3.0927	(2,0, -166)	0.833	5.3404	(2,0, -95)	0.834	19.6736	(2,0, -25)	0.838
4.8935	(1,0, -60)	0.501	3.1116	(2,0, -165)	0.833	5.3966	(2,0, -94)	0.834	20.4980	(2,0, -24)	0.838
4.9762	(1,0, -59)	0.501	3.1305	(2,0, -164)	0.833	5.4543	(2,0, -93)	0.834	21.4025	(2,0, -23)	0.839
5.0611	(1,0, -58)	0.501	3.1495	(2,0, -163)	0.833	5.5135	(2,0, -92)	0.834	22.3802	(2,0, -22)	0.839
5.1481	(1,0, -57)	0.501	3.1686	(2,0, -162)	0.833	5.5738	(2,0, -91)	0.834	23.4012	(2,0, -21)	0.839
5.2378	(1,0, -56)	0.501	3.1881	(2,0, -161)	0.833	5.6349	(2,0, -90)	0.834	24.3823	(2,0, -20)	0.839
5.3313	(1,0, -55)	0.501	3.2080	(2,0, -160)	0.833	5.6968	(2,0, -89)	0.834	25.3580	(2,0, -19)	0.840
5.4291	(1,0, -54)	0.501	3.2283	(2,0, -159)	0.834	5.7597	(2,0, -89)	0.834	26.5740	(2,0, -18)	0.841
5.5310	(1,0, -53)	0.501	3.2490	(2,0, -158)	0.834	5.8240	(2,0, -88)	0.834	28.0605	(2,0, -17)	0.842
5.6370	(1,0, -52)	0.501	3.2699	(2,0, -157)	0.834	5.8903	(2,0, -87)	0.834	29.7907	(2,0, -16)	0.842
5.7468	(1,0, -51)	0.501	3.2908	(2,0, -156)	0.834	5.9587	(2,0, -86)	0.834	31.7772	(2,0, -15)	0.843
5.8606	(1,0, -50)	0.501	3.3118	(2,0, -155)	0.834	6.0291	(2,0, -85)	0.834	34.0521	(2,0, -14)	0.844
5.9793	(1,0, -49)	0.502	3.3329	(2,0, -154)	0.834	6.1012	(2,0, -84)	0.834	36.6456	(2,0, -13)	0.845
6.1033	(1,0, -48)	0.502	3.3545	(2,0, -153)	0.834	6.1742	(2,0, -83)	0.834	39.5333	(2,0, -12)	0.845
6.2326	(1,0, -47)	0.502	3.3765	(2,0, -152)	0.834	6.2478	(2,0, -82)	0.834	42.4434	(2,0, -11)	0.844
6.3670	(1,0, -46)	0.502	3.3991	(2,0, -151)	0.834	6.3222	(2,0, -81)	0.834	45.3309	(2,0, -10)	0.845
6.5066	(1,0, -45)	0.502	3.4221	(2,0, -150)	0.834	6.3985	(2,0, -80)	0.834	49.3875	(2,0, -9)	0.848
6.6513	(1,0, -44)	0.502	3.4453	(2,0, -149)	0.834	6.4776	(2,0, -79)	0.834	55.0127	(2,0, -8)	0.850
6.8019	(1,0, -43)	0.502	3.4687	(2,0, -148)	0.834	6.5598	(2,0, -78)	0.834	62.4566	(2,0, -7)	0.851
6.9599	(1,0, -42)	0.502	3.4921	(2,0, -147)	0.834	6.6445	(2,0, -77)	0.834	72.4121	(2,0, -6)	0.852
7.1269	(1,0, -41)	0.502	3.5156	(2,0, -146)	0.834	6.7314	(2,0, -76)	0.834	86.0599	(2,0, -5)	0.851
7.3048	(1,0, -40)	0.502	3.5395	(2,0, -145)	0.834	6.8195	(2,0, -75)	0.834	105.4720	(2,0, -4)	0.844
7.4943	(1,0, -39)	0.502	3.5640	(2,0, -144)	0.834	6.9084	(2,0, -74)	0.834	134.5426	(2,0, -3)	0.821
7.6950	(1,0, -38)	0.502	3.5892	(2,0, -143)	0.834	6.9984	(2,0, -73)	0.834	176.8873	(2,0, -2)	0.804
7.9052	(1,0, -37)	0.503	3.6148	(2,0, -142)	0.834	7.0908	(2,0, -72)	0.834	208.5777	(2,0, -1)	0.982
8.1217	(1,0, -36)	0.503	3.6409	(2,0, -141)	0.834	7.1870	(2,0, -71)	0.834	250.1862	(2,1, -1)	0.894
8.3402	(1,0, -35)	0.503	3.6672	(2,0, -140)	0.834	7.2871	(2,0, -70)	0.834	289.4570	(2,2, -1)	0.868
8.5616	(1,0, -34)	0.503	3.6936	(2,0, -139)	0.834	7.3910	(2,0, -69)	0.834	313.7516	(2,2, 0)	0.901
8.7984	(1,0, -33)	0.503	3.7200	(2,0, -138)	0.834	7.4981	(2,0, -68)	0.834	357.6327	(2,3, 0)	0.887

TABLE 5

COMPARISON BETWEEN MODEL FREQUENCIES OF THE BEST-FITTING MODEL AND THE δ SCUTI FREQUENCIES. ν_{obs} IS THE OBSERVED FREQUENCY AND ν_{mod} IS ITS CORRESPONDING MODEL FREQUENCY. (ℓ, n_p, n_g, m) ARE THE SPHERICAL HARMONIC DEGREE, THE RADIAL ORDERS IN P-MODE PROPAGATION ZONE, THE RADIAL ORDERS IN G-MODE PROPAGATION ZONE, AND THE AZIMUTHAL NUMBER OF THE MODEL FREQUENCY, RESPECTIVELY. $|\nu_{\text{obs}} - \nu_{\text{mod}}|$ REPRESENTS THE FREQUENCY DIFFERENCE BETWEEN THE OBSERVED FREQUENCY AND ITS MODEL COUNTERPART.

ID	ν_{obs} (μHz)	ν_{mod} (μHz)	(ℓ, n_p, n_g, m)	$ \nu_{\text{obs}} - \nu_{\text{mod}} $ (μHz)
<i>F</i>	196.531	196.258	(0, 0, 0, 0)	0.273
<i>p</i> ₁	188.113	188.316	(1, 0,-1,-1)	0.203
<i>p</i> ₂	253.138	253.333	(0, 1, 0, 0)	0.195
<i>p</i> ₃	203.149	203.033	(2, 0,-1,-2)	0.116
<i>p</i> ₄	250.061	250.186	(2, 1,-1, 0)	0.125
<i>p</i> ₅	203.326	203.309	(1, 1,-1, 0)	0.017
<i>p</i> ₆	308.669	308.665	(2, 2, 0,-2)	0.004
<i>p</i> ₇	252.825	252.710	(2, 1,-1,+1)	0.115

TABLE 6

COMPARISON BETWEEN MODEL FREQUENCIES OF THE BEST-FITTING MODEL AND THE γ DOR FREQUENCIES. ν_{obs} AND P_{obs} REPRESENT THE FREQUENCY AND PERIOD OF THE OBSERVED MODES, RESPECTIVELY. P_{mod} IS THE PERIOD OF ITS MODEL COUNTERPART. (ℓ, n_p, n_g, m) ARE THE SPHERICAL HARMONIC DEGREE, THE RADIAL ORDERS IN P-MODE PROPAGATION ZONE, THE RADIAL ORDERS IN G-MODE PROPAGATION ZONE, AND THE AZIMUTHAL NUMBER OF THE MODEL FREQUENCY, RESPECTIVELY. $|P_{\text{obs}} - P_{\text{mod}}|$ REPRESENTS THE PERIOD DIFFERENCE BETWEEN THE OBSERVATION AND ITS MODEL COUNTERPART.

ID	ν_{obs} (d^{-1})	P_{obs} (days)	P_{mod} (days)	(ℓ, n_p, n_g, m)	$ P_{\text{obs}} - P_{\text{mod}} $ (days)	ID	ν_{obs} (d^{-1})	P_{obs} (days)	P_{mod} (days)	(ℓ, n_p, n_g, m)	$ P_{\text{obs}} - P_{\text{mod}} $ (days)
<i>f</i> ₁	1.5954	0.6268	0.6278	(1,0,-15, 0)	0.0010	<i>f</i> ₃₃	0.8183	1.2220	1.2237	(2,0,-108, 2)	0.0017
<i>f</i> ₂	1.4342	0.6973	0.6985	(2,0,-26,-1)	0.0012	<i>f</i> ₃₄	0.5610	1.7825	1.7822	(2,0,-124, 1)	0.0003
<i>f</i> ₃	1.3660	0.7321	0.7307	(1,0,-15,-1)	0.0014	<i>f</i> ₃₅	3.6095	0.2770	0.2761	(2,0,-12, 1)	0.0009
<i>f</i> ₄	1.6903	0.5916	0.5906	(2,0,-29, 1)	0.0010	<i>f</i> ₃₆	0.5274	1.8961	1.8964	(1,0,-48, 0)	0.0003
<i>f</i> ₅	1.7974	0.5564	0.5542	(2,0,-31, 2)	0.0022	<i>f</i> ₃₇	0.3865	2.5873	2.5921	(2,0,-75, -1)	0.0048
<i>f</i> ₆	1.2488	0.8008	0.7998	(2,0,-52, 2)	0.0010	<i>f</i> ₃₈	2.6154	0.3824	0.3824	(1,0,-9, 1)	0.0000
<i>f</i> ₇	1.1984	0.8344	0.8346	(2,0,-44, 1)	0.0002	<i>f</i> ₃₉	1.3037	0.7670	0.7683	(2,0,-49, 2)	0.0013
<i>f</i> ₈	1.9165	0.5218	0.5252	(2,0,-25, 1)	0.0034	<i>f</i> ₄₀	0.6158	1.6239	1.6240	(1,0,-41, 0)	0.0001
<i>f</i> ₉	0.4515	2.2148	2.2119	(2,0,-97, 0)	0.0029	<i>f</i> ₄₁	0.7402	1.3510	1.3508	(2,0,-133, 2)	0.0002
<i>f</i> ₁₀	0.8973	1.1145	1.1123	(2,0,-89, 2)	0.0022	<i>f</i> ₄₂	0.4068	2.4582	2.4595	(2,0,-109, 0)	0.0013
<i>f</i> ₁₁	2.2015	0.4542	0.4564	(2,0,-19, 0)	0.0022	<i>f</i> ₄₃	0.5713	1.7504	1.7546	(2,0,-121, 1)	0.0042
<i>f</i> ₁₂	0.7279	1.3738	1.3732	(2,0,-138, 2)	0.0006	<i>f</i> ₄₄	0.3716	2.6911	2.6978	(2,0,-77, -1)	0.0067
<i>f</i> ₁₃	0.7501	1.3332	1.3340	(2,0,-81, 1)	0.0008	<i>f</i> ₄₅	0.3969	2.5195	2.5186	(1,0,-92, 1)	0.0009
<i>f</i> ₁₄	0.4298	2.3267	2.3259	(1,0,-59, 0)	0.0008	<i>f</i> ₄₆	1.5079	0.6632	0.6667	(2,0,-40, 2)	0.0035
<i>f</i> ₁₅	0.4600	2.1739	2.1710	(1,0,-55, 0)	0.0029	<i>f</i> ₄₇	2.4495	0.4082	0.4113	(2,0,-21, 2)	0.0031
<i>f</i> ₁₆	0.8429	1.1864	1.1862	(2,0,-52, 0)	0.0002	<i>f</i> ₄₈	1.8449	0.5420	0.5408	(2,0,-23, 0)	0.0012
<i>f</i> ₁₇	0.7658	1.3058	1.3036	(1,0,-28,-1)	0.0022	<i>f</i> ₄₉	0.3236	3.0902	3.0891	(2,0,-137, 0)	0.0011
<i>f</i> ₁₈	0.9521	1.0503	1.0503	(2,0,-46, 0)	0.0000	<i>f</i> ₅₀	2.4030	0.4161	0.4153	(1,0,-10, 1)	0.0008
<i>f</i> ₁₉	0.3067	3.2605	3.2699	(2,0,-145, 0)	0.0094	<i>f</i> ₅₁	0.4693	2.1308	2.1316	(2,0,-50, -2)	0.0008
<i>f</i> ₂₀	2.0490	0.4880	0.4890	(2,0,-26, 2)	0.0010	<i>f</i> ₅₂	0.2995	3.3389	3.3367	(2,0,-148, 0)	0.0022
<i>f</i> ₂₁	0.4440	2.2523	2.2501	(2,0,-68,-1)	0.0022	<i>f</i> ₅₃	1.6708	0.5985	0.5931	(2,0,-34, 2)	0.0054
<i>f</i> ₂₂	0.3118	3.2072	3.2075	(1,0,-82, 0)	0.0003	<i>f</i> ₅₄	0.5381	1.8584	1.8585	(1,0,-61, 1)	0.0001
<i>f</i> ₂₃	1.1048	0.9051	0.9056	(2,0,-63, 2)	0.0005	<i>f</i> ₅₅	1.0641	0.9398	0.9397	(2,0,-67, 2)	0.0001
<i>f</i> ₂₄	0.6325	1.5810	1.5792	(2,0,-42,-2)	0.0018	<i>f</i> ₅₆	3.6421	0.2746	0.2727	(2,0,-11, 0)	0.0019
<i>f</i> ₂₅	0.4757	2.1022	2.1005	(1,0,-72, 1)	0.0017	<i>f</i> ₅₇	3.0996	0.3226	0.3177	(2,0,-14, 1)	0.0049
<i>f</i> ₂₆	0.9242	1.0820	1.0830	(2,0,-61, 1)	0.0010	<i>f</i> ₅₈	0.3385	2.9542	2.9548	(1,0,-55, -1)	0.0006
<i>f</i> ₂₇	0.6987	1.4312	1.4315	(2,0,-152, 2)	0.0003	<i>f</i> ₅₉	0.6639	1.5063	1.5041	(1,0,-38, 0)	0.0022
<i>f</i> ₂₈	0.8367	1.1952	1.1949	(2,0,-42,-1)	0.0003	<i>f</i> ₆₀	0.8310	1.2034	1.2006	(2,0,-103, 2)	0.0028
<i>f</i> ₂₉	0.6826	1.4650	1.4641	(1,0,-37, 0)	0.0009	<i>f</i> ₆₁	2.4595	0.4066	0.4017	(1,0,-9, 0)	0.0049
<i>f</i> ₃₀	0.8004	1.2494	1.2495	(2,0,-74, 1)	0.0001	<i>f</i> ₆₂	0.6064	1.6491	1.6493	(2,0,-110, 1)	0.0002
<i>f</i> ₃₁	0.5989	1.6697	1.6689	(2,0,-112, 1)	0.0008	<i>f</i> ₆₃	0.4968	2.0129	2.0140	(1,0,-51, 0)	0.0011
<i>f</i> ₃₂	1.1283	0.8863	0.8875	(2,0,-61, 2)	0.0012						